

# Intrinsically disordered region of Talin's FERM domain functions as an initial PIP<sub>2</sub> recognition site

Jannik Buhr

Florian Franz

Frauke Gräter

June 24, 2022

Focal adhesions mediate the interaction of the cytoskeleton with the extracellular matrix (ECM). Cell-ECM adhesion is used by almost all cells both during development and homeostasis and ranges from dynamic to permanent. As such, it is an important process in health and disease alike. Talin is a central regulator and adaptor protein of the multiprotein focal adhesion complexes and is responsible for integrin activation and force-sensing. We evaluated direct interactions of talin with the membrane lipid phosphatidylinositol 4,5-bisphosphate (PIP<sub>2</sub>) by means of molecular dynamics simulations. A newly published autoinhibitory structure of talin, where common PIP<sub>2</sub> interaction sites are covered up, sparked our curiosity for a hitherto less examined loop as a potential site of first contact. We show that this unstructured loop in the F1 subdomain of the Talin1 FERM domain is able to interact with PIP<sub>2</sub> and can facilitate further interactions by serving as a flexible membrane anchor. This work presents the dynamics of the interaction and identifies key residues. Further, we surveyed the effect of a physiological PIP<sub>2</sub> enrichment at focal adhesion sites on the dynamics of talin through force-probe molecular dynamics simulations. The results provide backing for the direct involvement of PIP<sub>2</sub> in the localization and activation of talin.



This is a draft and as such subject to change.

## 💡 Tip

You can find the poster that goes along with the paper presented at the [Annual Meeting of the Biophysical Society 2022](#) in your favorite format here: [web/html](#), [print/pdf](#). The source repository for this paper lives [here](#). The preliminary and less feature-rich pdf version lives [here](#).

## Introduction

It is critical for cells to mechanically sense their surroundings at cell adhesion sites for a multitude of biological processes. Contact with the extracellular matrix and surrounding cells regulates growth, differentiation, motility and even apoptosis (1–4). The multiprotein focal adhesion complex is responsible for translating between biochemical and mechanical signals, where both directions, outside-in and inside-out activation, are being investigated (5, 6).

At the center of the focal adhesion complex sits the adaptor protein talin, which dynamically unfolds and refolds under force (7). A schematic of Talin can be seen in Figure 1a. Through interaction with integrin tails (dark green) (8), which in turn interact with collagen fibers via their heads, it links the extracellular matrix to the intracellular cytoskeleton by directly interacting with actin. Talin also features specific interactions with the membrane. Their formation, mechanical stability and role in mechanosensing remain to be fully resolved.

Talin features an N-terminal FERM domain (F for 4.1 protein, E for ezrin, R for radixin and M for moesin), which is composed of the subdomains F0 to F3 and provides a link to the cytosolic side of the plasma membrane (9). It does so via a conserved binding motif for phosphatidylinositol 4,5-bisphosphate ( $\text{PIP}_2$ ), which is enriched at active focal adhesion sites (10–12). The main  $\text{PIP}_2$  binding sites are located in F2 and F3 (highlighted as red spheres in Figure 1a). Notably, the Talin1 FERM domain differs from other FERM proteins through the addition of the F0 subdomain, which is connected to F1 via a charged interface, as well as an insertion in F1, a flexible loop with helical propensity and basic residues (13).

Additionally, Talin's FERM domain exists in an extended conformation, as opposed to the cloverleaf-like conformation of other FERM proteins (14). F3 also has a binding site for  $\beta$ -integrin tails (15) and is partly responsible for the enrichment of  $\text{PIP}_2$  at the membrane through a binding site for PIPK $\gamma$  (16). A second integrin binding site is located with the rod domain 11 (R11) (17). Talin interacts with the cytoskeleton through actin binding sites (F2-F3, R4-R8, R13-DH) (18). The review by Klapholz et al. (19) provides an excellent overview of the many interaction sites of talin and its central role in the focal adhesion complex.

The mechanistic role of the disordered F1 loop in the many aspects of Talin function remains elusive. Its overall positive charge renders it a prime candidate as a  $\text{PIP}_2$  binding site. However, previous studies only identified a minor role of the loop in  $\text{PIP}_2$  binding compared to F2-F3 (20,

21). On the other hand, the F1 loop has been shown to contribute to talin-mediated integrin activation (13).

It was previously shown that F3 can interact with R9, which impedes integrin activation (22). Furthermore, in a recently determined cryo-electron microscopy structure of autoinhibited Talin1, Dedden et al. (23) showed that the rod domains R9 and R12 shield the established PIP<sub>2</sub> binding surface and the integrin binding site in F3 (see Figure 1b, Figure 1c). This beckons the question how this autoinhibition can be resolved. Song et al. (12) previously investigated a fragment of talin consisting of F2-F3 and an inhibiting rod segment and suggested a pull-push mechanism, whereby negatively charged PIP<sub>2</sub> attracts its positively charged binding surface on F2-F3 and simultaneously repels the negatively charged surface of the inhibitive rod segment. However, this still leaves open the question of how talin can establish a first contact with the membrane and remain within a sufficient proximity for this effect to kick in.

Here we test the hypothesis that the flexible F1 loop inserted into Talin's FERM domain serves as an additional PIP<sub>2</sub> interaction site that is readily accessible to PIP<sub>2</sub> even in Talin's autoinhibited conformation and further mechanically stabilizes Talin's interaction with the membrane. To this end, we modelled the loop, which due to its high flexibility, is not included in crystal structures of the FERM domain, such as PDB-ID 3IVF by Elliot et al. (14).

With a complete structure of the talin FERM domain we investigated the role of the F1 loop through molecular dynamics simulations, which had previously also proven useful to detect the recognition of PIP<sub>2</sub> in membranes by PH domains (24) or the FERM domain of Focal Adhesion Kinase (25).

In F0-F1 simulations, we found the loop to have a clear propensity to interact with the PIP<sub>2</sub>-containing membrane. Moreover, it is to be able to establish a first contact with the membrane even from unfavorable initial orientations due to its large search volume. Furthermore, we show with simulations of the full-length FERM domain that once the loop has established an initial contact, it can anchor the FERM domain to the membrane and establish the known major binding sites in F2-F3.

These results provide mechanistic insight into the role of membrane interactions for the localization of Talin at the center of the focal adhesion complex and highlight the role of secondary flexible binding surfaces for membrane recognition.

## Materials and Methods

### Molecular dynamics with GROMACS

Molecular dynamics simulations were performed with GROMACS (26, 27) version 2020.03 (28). A crystal structure of the Talin FERM domain by Elliot et al. (14) with the PDB-ID 3IVF was used as the basis of all simulations.

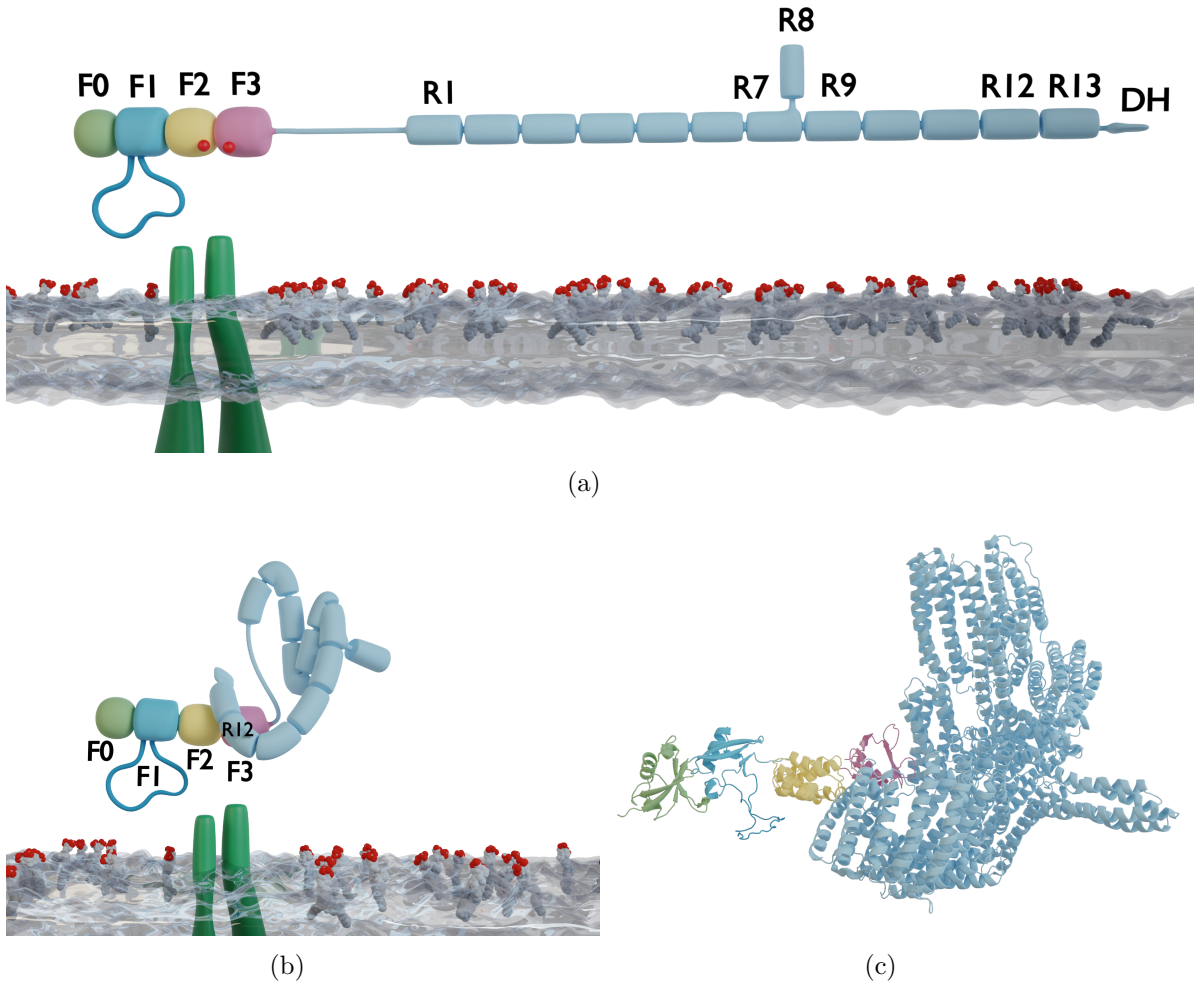


Figure 1: A schematic overview of Talin and our simulation setup. **a)** A schematic rendering of full-length Talin over a POPC membrane enriched with PIP<sub>2</sub> in the upper leaflet. The subdomains under scrutiny in this publication, namely F0-F3, which comprise the N-terminal FERM domain (or talin head) are highlighted in pastel colors (green, cyan, yellow, magenta). The two major PIP<sub>2</sub> binding sites in F2-F3 are marked with red spheres. An integrin binding site also resides in this area. Klapholz et al. (19) provide an excellent review of Talin’s central role in the focal adhesion complex and list further binding sites. The talin rod segments (or talin tail) are numbered R1 to R13. Note that under physiological conditions, with talin experiencing force from bound actin, the angle between the FERM domain and the talin rod would be more akin to 30° as opposed to the linear structure shown here for illustrative purposes. Tails of an integrin  $\alpha$  and  $\beta$  heterodimer reaching through the lipid bilayer are represented in green. **b)** A schematic rendering of the autoinhibited structure of Talin as crystallized by Dedden et al. (23) in combination with a cartoon representation in **c**). The completed FERM structure by Elliott et al. (14), with our addition of the modelled F1 loop, is fitted to the autoinhibited structure, as the latter does not include F0-F1 due to their flexibility. The complete FERM structure can be explored interactively in the context of our simulation system in Section . The main PIP<sub>2</sub>-binding sites in F2-F3 are occluded by rod domain 12<sup>4</sup>. Additionally, R9 covers up the integrin binding site.

The missing F1 domain loop between residues L133 and W144 was modeled using MODELLER (29, 30) via the interface to Chimera (31), followed by equilibration with GROMACS. The resulting conformation (see Section ) was compared to an NMR structure of the F1 domain (PDB-ID 2KC2) by Goult et al. (13).

The missing residue M1 was also added. The missing residues I399 and L400 were not modeled, leaving us with a continuous sequence from residue 1 to 398. Simulations were performed with the CHARMM36 force field. Topologies, including the membrane, were generated with the CHARMM-GUI web app (32–34) and GROMACS tools. All simulations used the TIP3P water model and were neutralized with 0.15 mol/L of NaCl. A 6-step equilibration was performed after gradient decent energy minimization while gradually relieving restraints on protein and membrane atoms. Production runs use a timestep of 2 fs, a Verlet cut-off scheme for Van-der-Waals interactions and the Particle Mesh Ewald (PME) method for long-range electrostatics. NTP-ensembles were achieved by Nosé-Hoover temperature coupling (35, 36) and Parrinello-Rahman pressure coupling (37). An example .mdp-file can be found in the supplementary materials in Section .

The initial equilibrium simulation of the completed FERM domain was run for 75 ns. Subsequently, the root mean squared fluctuation (RMSF) was calculated with GROMACS tools.

The F0F1 FERM sub domains (residues 1 to 197) were simulated to evaluate protein-membrane association using a rotational sampling approach. This entailed placing the protein 1.5 nm away from a 1-palmitoyl-2-oleoyl-glycero-3-phosphocholine (POPC) membrane in a total of 60 orientations spanning a rotation of 360 degrees. 6 replicates of each orientation were run for 200 ns each. However, due to a hardware failure, 6 of these 360 runs are only 50 to 150 ns long. Of the 119 lipids in the upper leaflet of the POPC membrane, 12 lipids were replaced with PIP<sub>2</sub>, which results in a physiological concentration of 10% PIP<sub>2</sub>.

From this rotational sampling, we selected representative conformations with loop-membrane interactions as the basis of 6 equilibrium simulations of the complete FERM domain over a POPC membrane with 26 PIP<sub>2</sub> lipids out of a total of 273 lipids in the upper leaflet. Each simulation ran for 400 ns. The initial conformations for perpendicular pulling simulations of the F0F1 subdomains to gauge interaction strength were also chosen from the rotational sampling set.

## Automation, Data Analysis and Availability

Setup scripts written in bash are available for all simulations shown in this work. Plots were generated with R using ggplot2 (38). Interactive structure representations are embedded using Mol\* (39). Schematic visualizations were rendered with blender (40) and VMD (41). Files relevant to this paper that are too big to be uploaded to this repository, such as trajectories and blender files, will be uploaded to a separate location.

This paper and the matching poster were generated with [quarto](#) (42) and Rmarkdown (43–45).

## Results

### The F1 loop can act as a point of first contact

The high flexibility of the F1 loop gave us the confidence to model it from sequence. It retained its flexibility in equilibrium simulations (Figure 5a), which in combination with comparisons to NMR structures (13) confirmed this approach. The resulting system that provides the basis for our simulations can be explored interactively in Section .

When simulating only F0-F1 over a POPC membrane containing 10% PIP<sub>2</sub>, we noticed that the F1 loop had a clear propensity to establish contact with the membrane. And once contact had been established the protein was anchored strongly enough for more contacts to evolve with time, pulling the protein onto the membrane (see Figure 2a, 2b, 2c). In order to control for a potential bias towards the loop as a result of the starting position we performed a rotational sampling of the system, where the starting angle of the loop with respect to the membrane was varied across 60 equally spaced angles. Figure 2d shows that independent of the starting position, the loop is able to find the membrane and bind to it, though this does happen earlier in the simulation when the loop starts favorably oriented towards the membrane (Figure 2e). However, even in its most unfavorable starting orientation (180°, oriented away from the membrane) the loop is able to find the membrane due to the large search space it can cover with its high flexibility (see Figure 5a).

Once contact has been made, it becomes exceedingly unlikely for F0-F1 to dissociate from the membrane (Figure 2f). Of 358 runs <sup>1</sup>, 89 runs never made contact with the membrane, but out of the 269 that did, only 10 eventually dissociated.

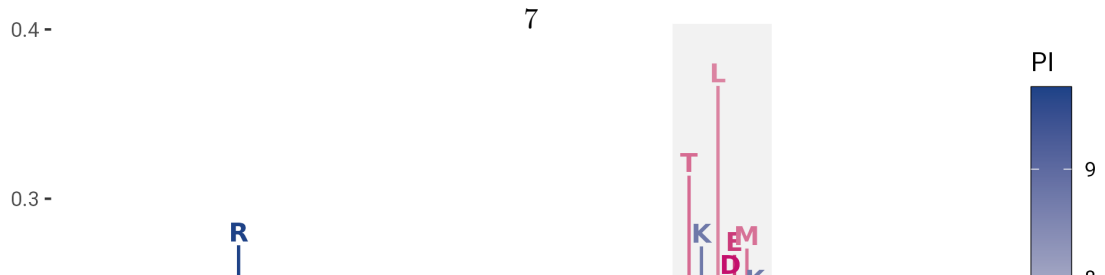
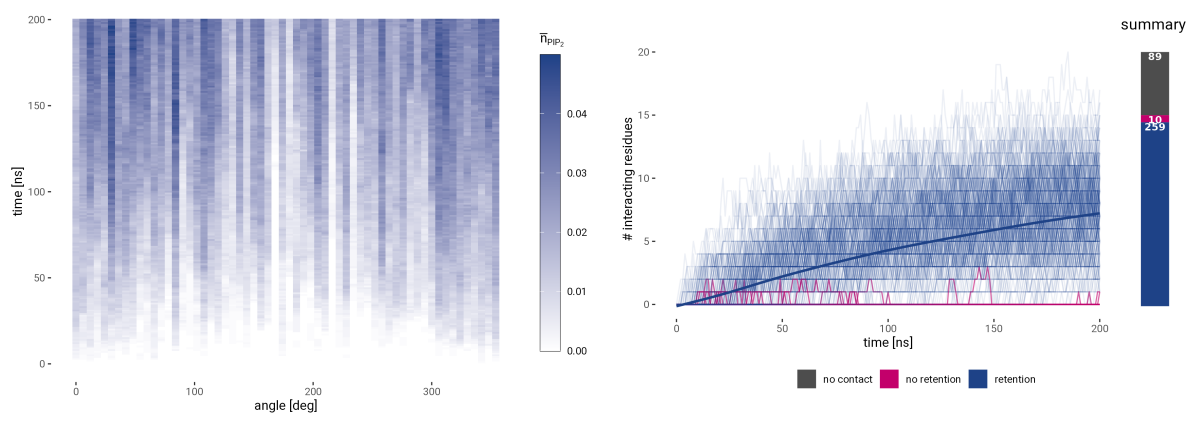
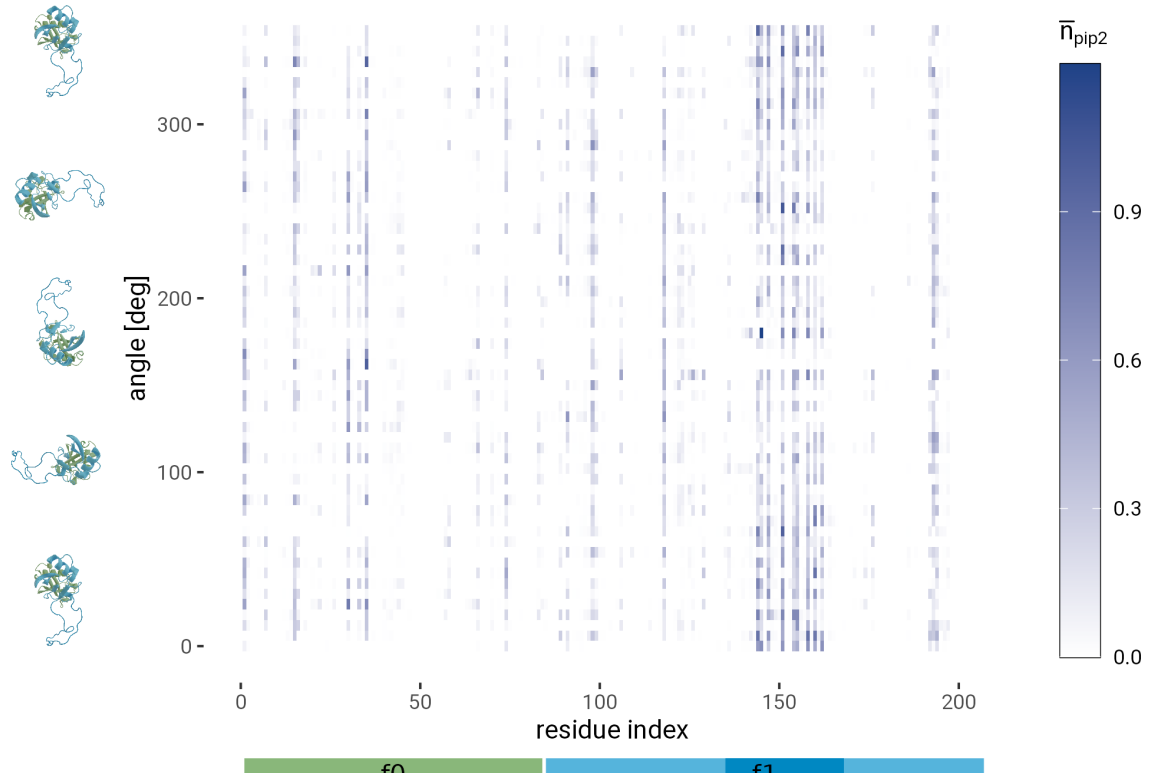
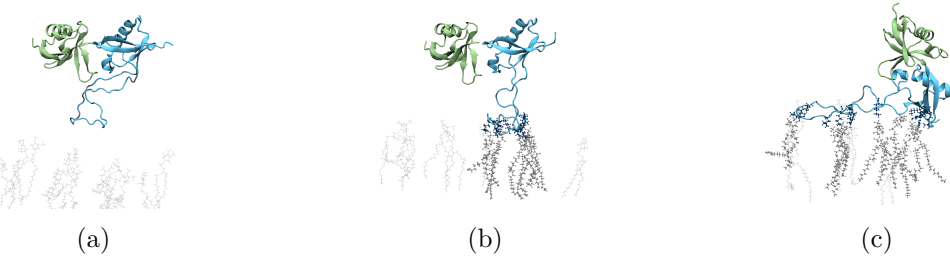
Figure 2g highlights the residues involved in the interaction.

### The F1 loop can facilitate further contacts

We chose a representative conformation from the rotational sampling as a starting point for force-probe simulations of F0-F1 perpendicular to the membrane to test the strength of the interaction (Figure 3b). An exemplary render of one of the simulations can be seen in Figure 3a. Pulling F0-F1 off the membrane requires peak forces of 100–120 pN, during which the interacting residues only very gradually loose contact (Figure 3c). This highlights the strong anchoring capabilities of the F1 loop. As seen in Figure 3d, during pulling residues not belonging to the F1 loop loose contact first, while the loop stays attached. The F1 loop works in conjunction with the F0 subdomain (see Figure 5d). Their high flexibility allows them to remain in contact with the membrane over large distances, which would allow for a spring-like re-establishing of more contacts should the force be alleviated.

---

<sup>1</sup>6 replicas each for 60 angles minus 2 runs lost to a storage failure



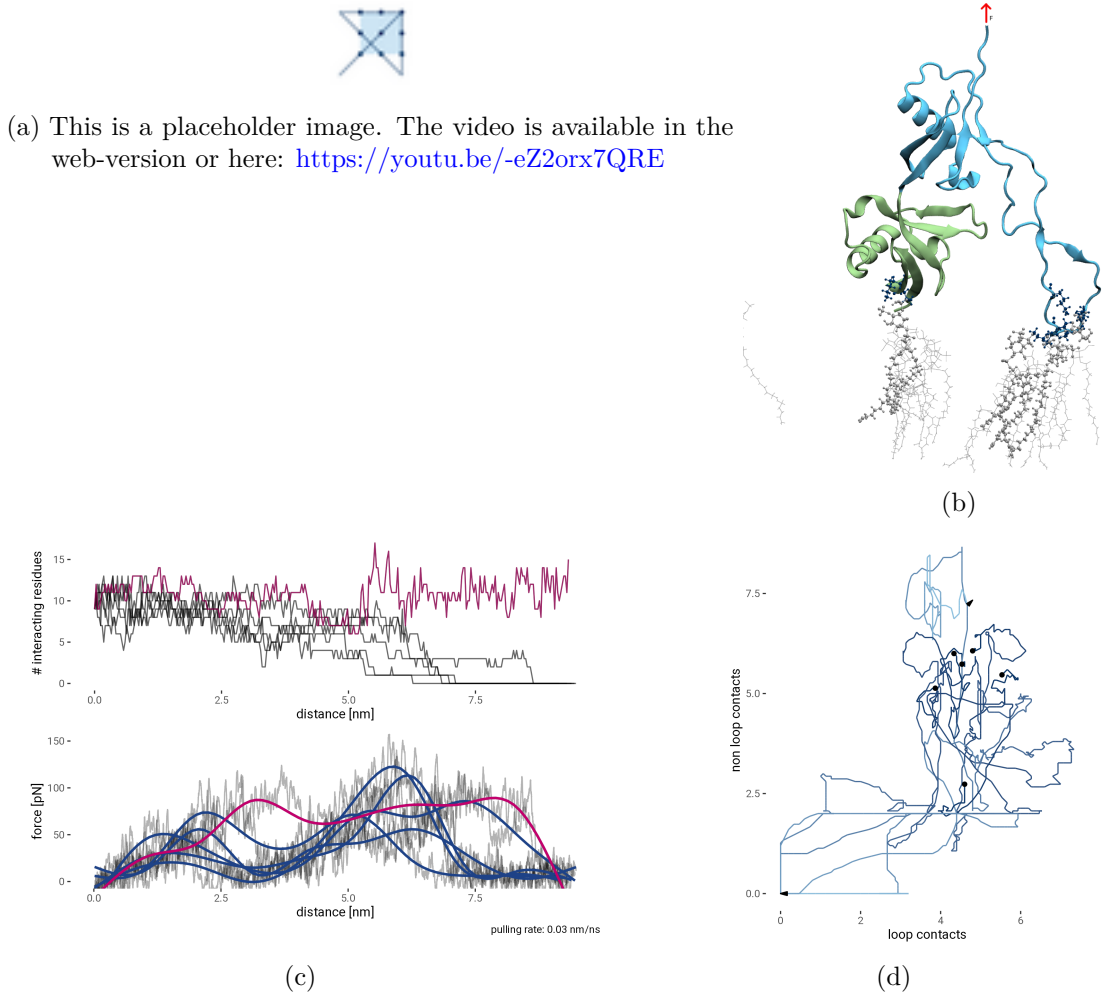


Figure 3: Vertical Pulling of F0-F1. **a)** A representative render of one of 6 force-probe MD simulations pulling F0-F1 off the membrane. It starts from a snapshot of F0-F1 in its bound conformation taken from the rotational sampling (Figure 2) and gets pulled upwards from its C-terminus. The direction of force is shown in the snapshot **b**). **c)** As F0-F1 gets pulled at a constant rate of 0.03 nm/ns we observe the time evolution of the force (bottom panel) and the number of interacting residues (top panel). The number of interacting residues goes down very gradually, as the high flexibility of loop allows the residues to remain in contact even as the distance increases. Replicat 4 is highlighted in magenta, as in this run the interactions were so strong that a total of 3 molecules of PIP<sub>2</sub> were pulled out of the membrane (1 by F0 and 2 by the F1 loop). A snapshot of this can be seen in Figure 5e. **d)** The time evolution of the number of contacts for residues belonging to the F1 loop and other residues shows how initially other residues loose contact until eventually the loop looses contacts as well. Lighter shades of blue correspond to a later time in the simulation. Black dots mark the starting positions. The longest remaining non-loop contacts belong to the N-terminus of F0 (for which **b** is also a representative snapshot), with the exception of replicate 4, as explained in **c**.

Simulations with the full-length FERM domain show that with the loop as an initial membrane contact, known PIP<sub>2</sub> binding sites can also be established (Figure 4a, Figure 4b). The highlighted residues include K272 of F2 and K316, K324, E342, and K343 of F3, which have been shown to be crucial for the membrane interaction of Talin and subsequent integrin activation by Chinthalapudi et al. (20).

## Discussion and Outlook

Using molecular dynamics simulations, we provide mechanistic insight into the membrane recognition dynamics of Talin. This adds a mode of interaction that helps to explain how Talin can find the membrane even when its main PIP<sub>2</sub> (and integrin) binding sites are blocked by autoinhibition. However, though we were able to conclusively show that the F1 loop is able to interact with the membrane even from most unfavorable positions, recognition this is only the first step. It would indeed be fascinating to also provide mechanistic ideas for the resolution of the autoinhibition by all-atom simulations of the FERM domain that also include an inhibiting rod segment. These larger-scale simulations might then be able to provide evidence for the push–pull mechanism proposed by Song et al. (12) or result in novel ideas.

## Author Contributions

Conceived and designed the experiments: JB FF FG. Performed the experiments: JB FF. Analyzed the data: JB FF. Contributed reagents/materials/analysis tools: FF. Wrote the paper: JB.

## Acknowledgments

This project has received funding from the European Research Council (ERC) under the European Union’s Horizon 2020 research and innovation programme (grant agreement No. 101002812).

This work was supported by the Klaus Tschira Foundation.

## Supplementary Material

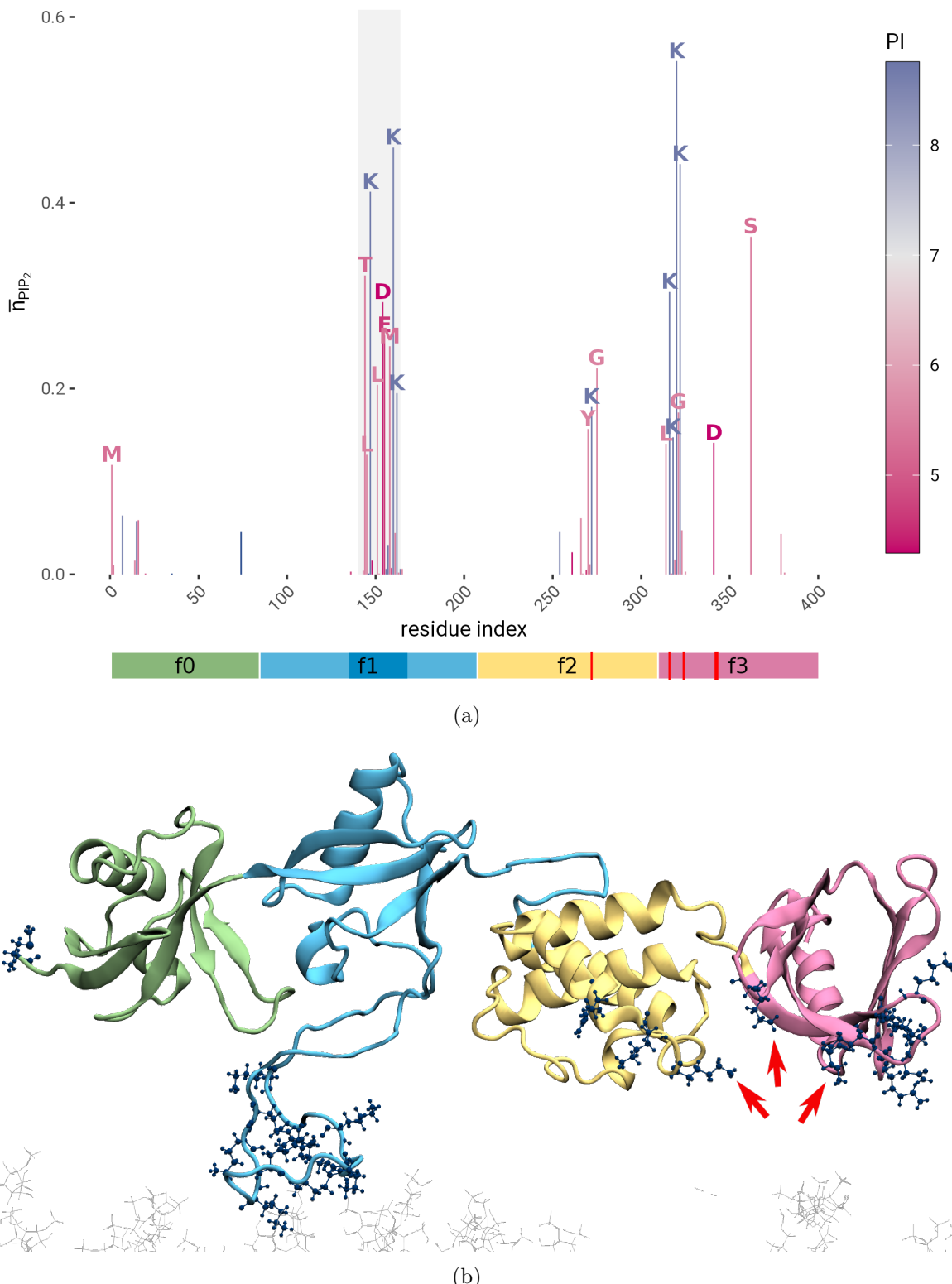
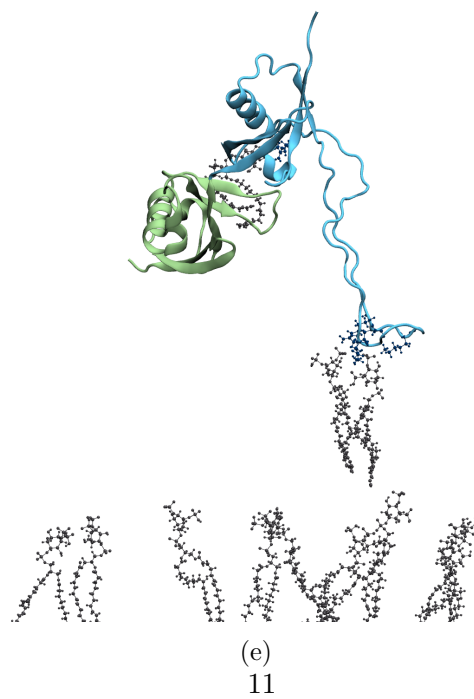
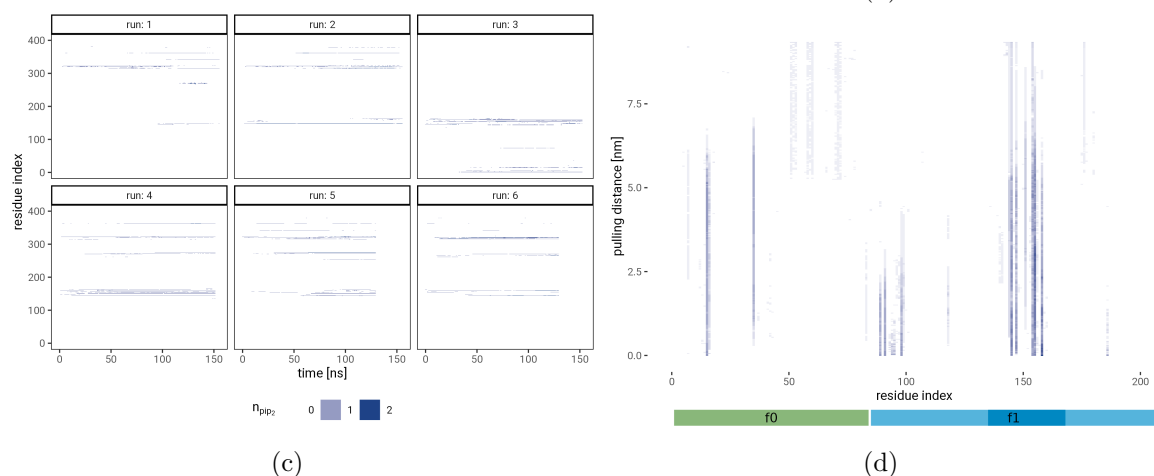
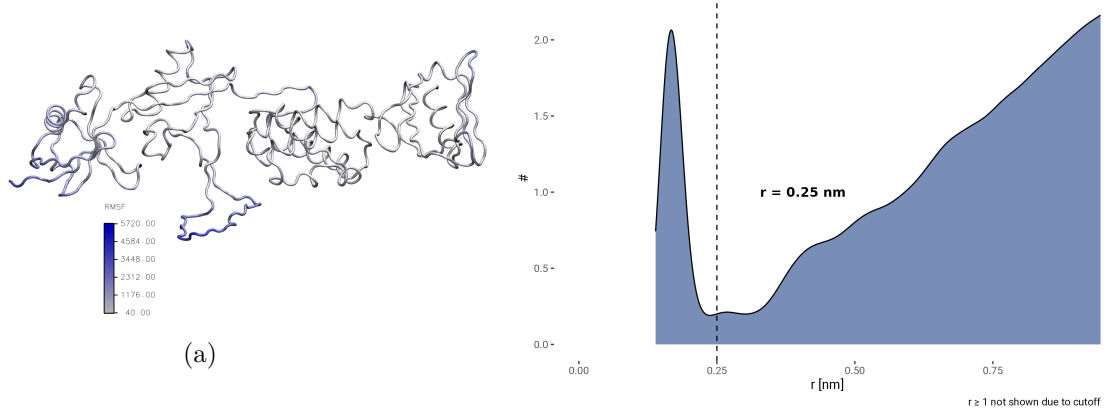


Figure 4: Simulation of the full-length FERM domain over a 10% PIP<sub>2</sub>-membrane. **a)** The Mean interaction scores of the individual  $\text{PIP}_2$  residues across 6 simulations. Color represents the isoelectric point of the amino acid in isolation (blue = basic, magenta = acidic). The known PIP<sub>2</sub> interaction sites K272 of F2 and K316, K324, E342, and K343 of F3 (20) are highlighted with red lines on the x-axis colorbar and can also be seen in the cartoon representation in **b)** where the main interacting residues are displayed as dark blue stick models.



11

Table 1: Top residues interacting with F0F1

Table 2: Top residues interacting with FERM

| Residue | Mean #PIP <sub>2</sub> | Residue | Mean #PIP <sub>2</sub> |
|---------|------------------------|---------|------------------------|
| M 1     | 0.188                  | M 1     | 0.118                  |
| K 15    | 0.184                  | T 144   | 0.322                  |

## Simulation system

### **i** Note

This interactive display is only available in the web version: <https://hits-mbm-dev.github.io/paper-talin-loop/>

## Scripts

### **i** Note

Analysis scripts, setup scripts and production trajectories will be uploaded and linked here.

## Production run parameters

```
integrator      = md
dt              = 0.002
nsteps          = 100000000
nstxout         = 5000
nstvout         = 5000
nstfout         = 50000
nstcalcenergy   = 100
nstenergy        = 1000
nstlog           = 1000
cutoff-scheme    = Verlet
nstlist          = 20
rlist            = 1.2
coulombtype     = pme
rcoulomb         = 1.2
vdwtype          = Cut-off
vdw-modifier     = Force-switch
rvdw_switch      = 1.0
rvdw             = 1.2
tcoupl           = Nose-Hoover
tc_grps          = SYSTEM
tau_t            = 1.0
ref_t            = 303.15
```

```

pcoupl          = Parrinello-Rahman
pcoupltype     = semiisotropic
tau_p          = 5.0
compressibility = 4.5e-5 4.5e-5
ref_p          = 1.0    1.0
constraints     = h-bonds
constraint_algorithm = LINCS
continuation     = yes
nstcomm         = 100
comm_mode        = linear
comm_grps        = SYSTEM
refcoord_scaling = com

```

1. Vogel, V., and M. Sheetz. 2006. [Local force and geometry sensing regulate cell functions](#). *Nature Reviews Molecular Cell Biology*. 7:265–275.
2. Oakes, P.W., and M.L. Gardel. 2014. [Stressing the limits of focal adhesion mechanosensitivity](#). *Current Opinion in Cell Biology*. 30:68–73.
3. Schiller, H.B., and R. Fässler. 2013. [Mechanosensitivity and compositional dynamics of cell–matrix adhesions](#). *EMBO reports*. 14:509–519.
4. Miroshnikova, Y.A., H.Q. Le, D. Schneider, T. Thalheim, M. Rübsam, N. Bremicker, J. Polleux, N. Kamprad, M. Tarantola, I. Wang, M. Balland, C.M. Niessen, J. Galle, and S.A. Wickström. 2018. [Adhesion forces and cortical tension couple cell proliferation and differentiation to drive epidermal stratification](#). *Nature Cell Biology*. 20:69–80.
5. Thamilselvan, V., and M.D. Basson. 2004. [Pressure activates colon cancer cell adhesion by inside-out focal adhesion complex and actin cytoskeletal signaling](#). *Gastroenterology*. 126:8–18.
6. Pelletier, A.J., T. Kunicki, Z.M. Ruggeri, and V. Quaranta. 1995. [The Activation State of the Integrin  \$\alpha\$ IIb \$\beta\$ 3 Affects Outside-in Signals Leading to Cell Spreading and Focal Adhesion Kinase Phosphorylation \\*](#). *Journal of Biological Chemistry*. 270:18133–18140.
7. Yao, M., B.T. Goult, B. Klapholz, X. Hu, C.P. Toseland, Y. Guo, P. Cong, M.P. Sheetz, and J. Yan. 2016. [The mechanical response of talin](#). *Nature Communications*. 7:11966.
8. Tadokoro, S., S.J. Shattil, K. Eto, V. Tai, R.C. Liddington, J.M. de Pereda, M.H. Ginsberg, and D.A. Calderwood. 2003. [Talin Binding to Integrin  \$\beta\$  Tails: A Final Common Step in Integrin Activation](#). *Science*. 302:103–106.
9. Chishti, A.H., A.C. Kim, S.M. Marfatia, M. Lutchman, M. Hanspal, H. Jindal, S.-C. Liu, P.S. Low, G.A. Rouleau, N. Mohandas, J.A. Chasis, J.G. Conboy, P. Gascard, Y. Takakuwa, S.-C. Huang, E.J.B. Jr, A. Bretscher, R.G. Fehon, J.F. Gusella, V. Ramesh, F. Solomon, V.T. Marchesi, S. Tsukita, S. Tsukita, M. Arpin, D. Louvard, N.K. Tonks, J.M. Anderson, A.S. Fanning, P.J. Bryant, D.F. Woods, and K.B. Hoover. 1998. [The FERM domain: A unique module involved in the linkage of cytoplasmic proteins to the membrane](#). *Trends in Biochemical Sciences*. 23:281–282.

10. Mani, T., R.F. Hennigan, L.A. Foster, D.G. Conrady, A.B. Herr, and W. Ip. 2011. **FERM Domain Phosphoinositide Binding Targets Merlin to the Membrane and Is Essential for Its Growth-Suppressive Function.** *Molecular and Cellular Biology*. 31:1983–1996.
11. Das, T., K. Safferling, S. Rausch, N. Grabe, H. Boehm, and J.P. Spatz. 2015. **A molecular mechanotransduction pathway regulates collective migration of epithelial cells.** *Nature Cell Biology*. 17:276–287.
12. Song, X., J. Yang, J. Hirbawi, S. Ye, H.D. Perera, E. Goksoy, P. Dwivedi, E.F. Plow, R. Zhang, and J. Qin. 2012. **A novel membrane-dependent on/off switch mechanism of talin FERM domain at sites of cell adhesion.** *Cell Research*. 22:1533–1545.
13. Goult, B.T., M. Bouaouina, P.R. Elliott, N. Bate, B. Patel, A.R. Gingras, J.G. Grossmann, G.C.K. Roberts, D.A. Calderwood, D.R. Critchley, and I.L. Barsukov. 2010. **Structure of a double ubiquitin-like domain in the talin head: A role in integrin activation.** *The EMBO Journal*. 29:1069–1080.
14. Elliott, P.R., B.T. Goult, P.M. Kopp, N. Bate, J.G. Grossmann, G.C.K. Roberts, D.R. Critchley, and I.L. Barsukov. 2010. **The Structure of the Talin Head Reveals a Novel Extended Conformation of the FERM Domain.** *Structure(London, England:1993)*. 18:1289–1299.
15. Calderwood, D.A., R. Zent, R. Grant, D.J.G. Rees, R.O. Hynes, and M.H. Ginsberg. 1999. **The Talin Head Domain Binds to Integrin  $\beta$  Subunit Cytoplasmic Tails and Regulates Integrin Activation \*.** *Journal of Biological Chemistry*. 274:28071–28074.
16. Calderwood, D.A., I.D. Campbell, and D.R. Critchley. 2013. **Talins and kindlins: Partners in integrin-mediated adhesion.** *Nature Reviews Molecular Cell Biology*. 14:503–517.
17. Horwitz, A., K. Duggan, C. Buck, M.C. Beckerle, and K. Burridge. 1986. **Interaction of plasma membrane fibronectin receptor with talin—a transmembrane linkage.** *Nature*. 320:531–533.
18. McCann, R.O., and S.W. Craig. 1997. **The I/LWEQ module: A conserved sequence that signifies F-actin binding in functionally diverse proteins from yeast to mammals.** *Proceedings of the National Academy of Sciences*. 94:5679–5684.
19. Klapholz, B., and N.H. Brown. 2017. **Talin – the master of integrin adhesions.** *Journal of Cell Science*. 130:2435–2446.
20. Chinthalapudi, K., E.S. Rangarajan, and T. Izard. 2018. **The interaction of talin with the cell membrane is essential for integrin activation and focal adhesion formation.** *Proceedings of the National Academy of Sciences of the United States of America*. 115:10339–10344.
21. Saltel, F., E. Mortier, V.P. Hytönen, M.-C. Jacquier, P. Zimmermann, V. Vogel, W. Liu, and B. Wehrle-Haller. 2009. **New PI(4,5)P<sub>2</sub>- and membrane proximal integrin-binding motifs in the talin head control B3-integrin clustering.** *Journal of Cell Biology*. 187:715–731.
22. Banno, A., B.T. Goult, H. Lee, N. Bate, D.R. Critchley, and M.H. Ginsberg. 2012. **Subcellular Localization of Talin Is Regulated by Inter-domain Interactions \*.** *Journal of Biological Chemistry*. 287:13799–13812.

23. Dedden, D., S. Schumacher, C.F. Kelley, M. Zacharias, C. Biertümpfel, R. Fässler, and N. Mizuno. 2019. [The Architecture of Talin1 Reveals an Autoinhibition Mechanism](#). *Cell.* 179:120–131.e13.
24. Buyan, A., A.C. Kalli, and M.S.P. Sansom. 2016. [Multiscale Simulations Suggest a Mechanism for the Association of the Dok7 PH Domain with PIP-Containing Membranes](#). *PLOS Computational Biology.* 12:e1005028.
25. Zhou, J., C. Aponte-Santamaría, S. Sturm, J.T. Bullerjahn, A. Bronowska, and F. Gräter. 2015. [Mechanism of Focal Adhesion Kinase Mechanosensing](#). *PLOS Computational Biology.* 11:e1004593.
26. Berendsen, H.J.C., D. van der Spoel, and R. van Drunen. 1995. [GROMACS: A message-passing parallel molecular dynamics implementation](#). *Computer Physics Communications.* 91:43–56.
27. Abraham, M.J., T. Murtola, R. Schulz, S. Páll, J.C. Smith, B. Hess, and E. Lindahl. 2015. [GROMACS: High performance molecular simulations through multi-level parallelism from laptops to supercomputers](#). *SoftwareX.* 1–2:19–25.
28. Lindahl, Abraham, Hess, and van der Spoel. 2020-01-01, 2020-01. [GROMACS 2020 source code](#). Zenodo.
29. Martí-Renom, M.A., A.C. Stuart, A. Fiser, R. Sánchez, F. Melo, and A. Sali. 2000. [Comparative protein structure modeling of genes and genomes](#). *Annual Review of Biophysics and Biomolecular Structure.* 29:291–325.
30. Webb, B., and A. Sali. 2016. [Comparative Protein Structure Modeling Using MOD-ELLER](#). *Current Protocols in Protein Science.* 86:2.9.1–2.9.37.
31. Pettersen, E.F., T.D. Goddard, C.C. Huang, G.S. Couch, D.M. Greenblatt, E.C. Meng, and T.E. Ferrin. 2004. [UCSF Chimera—a visualization system for exploratory research and analysis](#). *Journal of Computational Chemistry.* 25:1605–1612.
32. Brooks, B.R., C.L. Brooks, A.D. Mackerell, L. Nilsson, R.J. Petrella, B. Roux, Y. Won, G. Archontis, C. Bartels, S. Boresch, A. Caflisch, L. Caves, Q. Cui, A.R. Dinner, M. Feig, S. Fischer, J. Gao, M. Hodoscek, W. Im, K. Kuczera, T. Lazaridis, J. Ma, V. Ovchinnikov, E. Paci, R.W. Pastor, C.B. Post, J.Z. Pu, M. Schaefer, B. Tidor, R.M. Venable, H.L. Woodcock, X. Wu, W. Yang, D.M. York, and M. Karplus. 2009. [CHARMM: The biomolecular simulation program](#). *Journal of Computational Chemistry.* 30:1545–1614.
33. Jo, S., T. Kim, V.G. Iyer, and W. Im. 2008. [CHARMM-GUI: A web-based graphical user interface for CHARMM](#). *Journal of Computational Chemistry.* 29:1859–1865.
34. Lee, J., X. Cheng, J.M. Swails, M.S. Yeom, P.K. Eastman, J.A. Lemkul, S. Wei, J. Buckner, J.C. Jeong, Y. Qi, S. Jo, V.S. Pande, D.A. Case, C.L. Brooks, A.D. MacKerell, J.B. Klauda, and W. Im. 2016. [CHARMM-GUI Input Generator for NAMD, GROMACS, AMBER, OpenMM, and CHARMM/OpenMM Simulations Using the CHARMM36 Additive Force Field](#). *Journal of Chemical Theory and Computation.* 12:405–413.

35. Hoover, W.G. 1985. Canonical dynamics: Equilibrium phase-space distributions. *Physical Review A*. 31:1695–1697.
36. Nosé, S. 1984. A unified formulation of the constant temperature molecular dynamics methods. *The Journal of Chemical Physics*. 81:511–519.
37. Parrinello, M., and A. Rahman. 1981. Polymorphic transitions in single crystals: A new molecular dynamics method. *Journal of Applied Physics*. 52:7182–7190.
38. Wickham, H. 2016. Ggplot2: Elegant graphics for data analysis. Springer-Verlag New York.
39. Sehnal, D., S. Bittrich, M. Deshpande, R. Svobodová, K. Berka, V. Bazgier, S. Velankar, S.K. Burley, J. Koča, and A.S. Rose. 2021. Mol\* Viewer: Modern web app for 3D visualization and analysis of large biomolecular structures. *Nucleic Acids Research*. 49:W431–W437.
40. Community, B.O. 2018. Blender - a 3D modelling and rendering package.
41. Humphrey, W., A. Dalke, and K. Schulten. 1996. VMD – Visual Molecular Dynamics. *Journal of Molecular Graphics*. 14:33–38.
42. Allaire, J.J., C. Teague, C. Scheidegger, Y. Xie, and C. Dervieux. 2022. Quarto.
43. Xie, Y., J.J. Allaire, and G. Grolemund. 2018. R markdown: The definitive guide. Boca Raton, Florida: Chapman and Hall/CRC.
44. Xie, Y. 2015. Dynamic documents with R and knitr. Second. Boca Raton, Florida: Chapman and Hall/CRC.
45. Aden-Buie, G. 2022. Betterposter: A better scientific poster.